Available online at www.sciencedirect.com

ScienceDirect

journal homepage: www.elsevier.com/locate/he

Optimisation and characterisation of graphene-based microporous layers for polymer electrolyte membrane fuel cells

F.C. Lee [a,*], M.S. Ismail [b], K. Zhang [c], D.B. Ingham [a], F. Aldakheel [d], K.J. Hughes [a,**], L. Ma [a], A. El-Kharouf [c], M. Pourkashanian [a,e]

[a] Energy 2050, Department of Mechanical Engineering, Faculty of Engineering, University of Sheffield, Sheffield, S3 7RD, United Kingdom
[b] School of Engineering, University of Hull, Hull, HU6 7RX, United Kingdom
[c] Birmingham Centre for Fuel Cell and Hydrogen Research, University of Birmingham, Edgbaston, Birmingham, B15 2TT, United Kingdom
[d] Kuwait Institute for Scientific Research, Shuwaikh, 13109, Kuwait
[e] Translational Energy Research Centre, University of Sheffield, Sheffield, S3 7RD, United Kingdom

HIGHLIGHTS

- Microporous layers were fabricated with varying weight inclusions of graphene.
- Composite MPLs were characterised by their morphology, microstructure and electrochemical properties.
- Lower graphene concentrations (30%) improved cell performance in low humidity conditions.
- Graphene concentration at 50 wt % or above enhances cell performance in high humidity conditions.

GRAPHICAL ABSTRACT

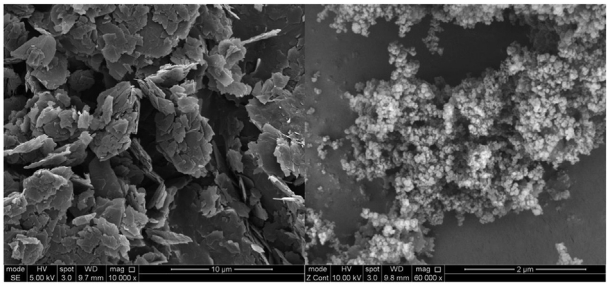

ARTICLE INFO

Article history:
Received 3 January 2023
Received in revised form
30 March 2023
Accepted 1 May 2023
Available online 18 May 2023

ABSTRACT

The viability of graphene-based microporous layers (MPLs) for polymer electrolyte membrane fuel cells is critically assessed through detailed characterisation of the morphology, microstructure, transport properties and electrochemical characterisation. Microporous layer composition was optimised by the fabrication of several hybrid MPLs produced from various ratios of graphene to Vulcan carbon black. Single cell tests were performed at various relative humidities between 25% and 100% at 80 °C, in order to provide a detailed understanding of the effect of the graphene-based MPL composition on the fuel cell

* *Corresponding author.*
** *Corresponding author.*
E-mail addresses: fclee1@sheffield.ac.uk, florenceclee91@gmail.com (F.C. Lee), k.j.hughes@sheffield.ac.uk (K.J. Hughes).
https://doi.org/10.1016/j.ijhydene.2023.05.003

Keywords:
Polymer electrolyte membrane fuel cells
Gas diffusion layers
Microporous layers
Graphene
Carbon black
Characterisation

performance. The inclusion of graphene in the MPL alters the pores size distribution of the layer and results in presence of higher amount of mesopores. Polarisation curves indicate that a small addition of graphene (i.e. 30 wt %) in the microporous layer improves the fuel cell performance under low humidity conditions (e.g. 25% relative humidity). On the other hand, under high humidity conditions (≥50% relative humidity), adding higher amounts of graphene (≥50 wt %) improves the fuel cell performance as it creates a good amount of mesopores required to drive excess water away from the cathode electrode, particularly when operating with high current densities.

Introduction

Polymer Electrolyte Membrane Fuel Cells (PEMFCs) are electrochemical energy conversion devices capable of providing clean and sustainable for transport, stationary and portable applications, owing to their high-power density, fast start-up time and operation at relatively low temperatures [1]. However, further research is required in order to improve their performance, durability and to reduce their cost. Water management remains one of the largest challenges facing the fuel cell technology especially at high current density; amount of water in the membrane electrode assembly (MEA) should be optimised to avoid either water flooding which limits reactant transport [2,3] or membrane dehydration which limits proton transport [4,5]. The microporous layer (MPL) within the gas diffusion layer (GDL) of PEFC is widely acknowledged as a crucial performance enhancing component [6,7], improving cell efficiency and durability through improved water management and better electrical contact with the catalyst layer [7].

The purpose of this research is to develop a greater understanding of how composition affects MPL microstructure and morphology, and ultimately identify strategies to improve fuel cell efficiency. The synergetic effect of different types of carbon has been explored by several researchers. Early research investigated the interactions of different types of carbon black when used together in the MPL, and the effects imparted on MPL morphology, gas transmission and liquid water saturation [8,9]. Numerous studies have examined the synergy between carbon nanotubes and high purity carbon black in the microporous layer; inclusions of multi-wall carbon nanotubes have influenced the microstructure and pore size distribution of the layer, and improved the mass transport phenomena particularly in saturated conditions [2,10–12]. Similar studies have been undertaken using graphene as an additive in the microporous layer [13,14]; these demonstrated that the addition of graphene can lead to significant improvements in MEA performance, resulting in higher power densities and limiting current densities. The performance enhancements with graphene were strongly influenced by the cell operating conditions, notably the temperature and relative humidity.

A recent trend has seen graphene being explored as an alternative to carbon black in the MPL. Graphene is a two-dimensional monolayer of graphitic carbon atoms, with good mechanical stiffness and elasticity, as well as extremely high electrical conductivity and thermal conductivity [15]. For these reasons graphene is an attractive material to use in PEM fuel cell components where high electron mobility and thermal conductivity are crucial. Consequently graphene has been researched as an additive to the gas diffusion layer [16], the membrane [17–19] and the bi-polar plates [20–22]. However, the most widely studied application of graphene is as a catalyst layer support [23–28], where the high electrical conductivity, the unique electron transfer characteristics and high surface area has precipitated a significant volume of research.

Graphene has previously been explored as an MPL material by a few researchers both as a freestanding MPL [14] and conventionally applied to carbon substrate [13,29–31]. Leeuwner et al. [14] fabricated a free-standing MPL for the cathode GDL from commercially available compressed 3D freestanding graphene foam. However, the lack of treatment with hydrophobic agent and inhomogeneous surface limited the power density at higher current densities (>1500 mA cm^{-2}) due to flooding. The majority of research into graphene microporous layers has used graphene nanoplatelets which are commercially available or have been produced in-house by electrochemistry as in Refs. [13,14,29]. Ozden et al. [30] fabricated and characterised MPLs produced from a commercial Grade DU25 graphene. The in-house graphene-based MPL exhibited a higher peak power density than the Vulcan carbon black-based MPLs at relative humidity ranging between of 40–100%. However, their research was limited by the use of a single material for the fabrication of the MPL, pure graphene; composite MPLs produced from graphene and carbon black were not considered. When explored in a later publication this was limited to a 1:1 ratio of the two materials. Mariani et al. [31] used various commercial graphene platelets as an MPL material, these were characterised in order to optimise the type of graphene used. They report that the 25 μm sized graphene platelets MPL produced the highest power density. Furthermore, MPLs were produced from combination of graphene and carbon black (1:1 ratio) the two materials were shown to have complimentary effect improving cell performance. Similar studies exfoliated graphene [13], reduced graphene oxide and natural graphite [29] indicate that composite MPLs produced from graphene and carbon black results in a higher current density particularly at higher relative humidity operation. Najafab et al. [13] manufactured graphene from electrochemical exfoliation, the resulting product was then used to produced MPLs which were characterised alongside conventional carbon black, and composite MPLs (1:1 ratio). Again the composite MPL produced from the two materials had an

enhanced performance, benefiting from reduced activation, ohmic and mass transport losses.

In the literature, there have been several publications comparing single cell performance between graphene and the conventional carbon black microporous layers, although there is an absence of data for the longevity of these MPLs [32,33]. An insightful analysis was undertaken by Latorrata et al. [33] who investigated the durability of graphene MPLs against those produced from carbon black, for both the anode and cathode GDL. An in depth analysis into the degradation of the MPLs was carried out by performing post-mortem ex-situ analysis on the samples, and repeated polarisation curves. Interestingly the MEAs with graphene-based MPLs reportedly showed reduced deterioration (i.e. fewer ohmic and concentration losses) due to the absence of surface cracks.

Although these works further our understanding of how graphene can be used in the MPL, they have not explored the optimisation of the ratio of graphene platelets to carbon black. Mixing graphene with carbon black, or a mixture of graphene with different morphologies has the potential for a synergetic effect on MPL morphology and microstructure, and thus optimising cell performance. Here we present the fabrication and characterisation of novel MPLs produced from graphene-based materials. The microporous layers were produced from a high purity graphene (Nanene), Vulcan XR72C carbon black, and a combination of the two materials. The MPLs were then characterised for their morphology, physical properties and fuel cell performance.

Methodology

Materials

The fabricated dual-layer GDLs were used at the cathode. The carbon substrate used to produce the dual-layer GDLs was Toray TGP H-60 carbon paper with 10% wt. PTFE (Fisher Scientific, UK). The carbon powder used in the MPL ink was Vulcan XC 72 R (Sigma Aldrich®, BET surface area: 238 $m^2 g^{-1}$ [34] whereas the few-layer graphene (FLG) powder used in this study was Nanene (2-DTech Ltd., UK). Nanene is produced using a mechanochemical process with BET surface area of 45 $m^2 g^{-1}$. The hydrophobicity of the layer was achieved by the addition of 60 wt % PTFE dispersion (Sigma-Aldrich®, UK).

MPLs were produced from a viscous ink consisting of carbon black and PTFE. Distilled water was used as the solvent for the MPL ink. Triton X-100 (Sigma Aldrich®, UK) and methyl cellulose (Sigma Aldrich®, UK) were added to improve the dispersibility and the rheology of the MPL ink [35]. The MPL was applied to commercial Toray TGP-H-60 GDL (10 wt % PTFE) using a micrometre applicator (Industrial Physics, UK) with a heated plate at 80 °C.

The MPL coated GDLs were heat treated in a tube furnace to thermally decompose the Triton ×100 and methyl cellulose, and to uniformly distribute the PTFE particles throughout the MPL. The temperature profile was 120 °C for 1 h, 280 °C for 30 min and 350 °C (sintering) for 30 min [36]. Table 1 lists all the MPL compositions investigated in the study following initial drying and thermal treatment. The MPL composition by weight remained unchanged consisting of 80% carbon and 20% PTFE. The carbon loading was kept constant at 2.0 mg/cm^2 in all MPLs as in Ref. [36].

Table 1 – The compositions of the microporous layers.

MPL	Vulcan (wt.%)	Nanene (wt.%)	PTFE (wt. %)
G0	80	0	20
G30	56	24	20
G50	40	40	20
G70	24	56	20
G100	0	80	20

The thickness of each of the GDL samples was measured using a micrometre before and after the MPL coating was applied. Each sample was measured at 5 equally spaced positions within it to provide a representative average value of the thickness.

SEM imaging

The morphological characteristics of the GDLs with different MPLs were observed using Scanning Electron Microscopy (SEM). All SEM imaging was performed on a JEOL instrument (Model JSM-6010LA). The obtained SEM images show the surface structure and morphology.

Porosity/pore size distribution

Mercury intrusion porosimetry (MIP) was used to obtain the pore characteristics of the blank and coated GDLs (pore size distribution and porosity). In this instance the measurements were conducted using a MicroActive AutoPore V 9600 V (Micrometrics, USA). The pore size distribution was obtained from the measured relationship between the intrusion pressure and the intruded volume of mercury at that pressure. As the intruded volume of mercury is correlated to pore volumes of specific diameters at each intrusion step.

Contact angle

The water contact angle of the GDL surface was measured using a video drop shape system FTA200 goniometer (First Ten Angstroms, USA). Owing to the slight inhomogeneity of the GDL surface, the contact angle measurements were taken at several positions on the surface of the sample to ensure a realistic representation of the average value. As such the contact angle was measured at 7 positions on the GDL sample, and the average value and the 95% confidence interval were then calculated.

Through-plane permeability

An in-house setup was used to measure the through-plane permeability, as documented in Refs. [37,38]. The setup consists of lower and upper fixtures, where a circular GDL sample of 25.4 mm in diameter is placed and tightened between two fixtures. Nitrogen gas is forced to flow through the sample, and the pressure drop is measured across the GDL for at least 5 flowrates. A flow controller (HFC-202, Teledyne Hastings, UK) with a range of 0.0–0.1 SLPM is used to control the flowrate of the nitrogen gas. A differential pressure sensor (PX653,

Omega, UK) with a range of ±12.5 Pa, was used to measure the pressure difference across the GDL sample.

Flow rates were very low and therefore the flow was assumed be laminar. This renders the inertial losses negligible and Darcy's Law can, therefore, be employed to calculate the gas permeability of the GDL samples [37]:

$$\frac{\Delta P}{L} = \frac{\mu}{k} v \tag{1}$$

$$v = \frac{Q}{\pi D^2/4} \tag{2}$$

where ΔP is the pressure drop across the sample, L is the measured thickness of the samples, μ is the dynamic viscosity of nitrogen (1.8×10^{-5} Pa s), k is the gas permeability of the sample, v is the velocity of the flowing gas, Q is the volumetric flow rate and D is the diameter of the sample exposed to the flow, respectively.

In-plane electrical conductivity

The experimental procedure was derived from the in-plane conductivity setup as described by Ismail et al. [39] based on [40]. The GDL sample was positioned on an insulating polycarbonate plate. As previously mentioned, the thickness of the GDL samples averaged from 5 measurements taken at equally spaced positions. The electrical resistance was measured by an RS Pro 804 Ohmmeter (RS Components, UK), which has a resolution of 0.01 mΩ. As the distance between the two voltage probes must be kept constant, they are housed in a plastic body, where spacing of which is equal to the width of the GDL sample (20 mm).

According to Smits' method, the correction factor is dependent on the dimensions of the GDL samples and the spacing between the probes. Essentially, it is derived from two ratios being, the length of the GDL to its width (a/d), and the width of the GDL to the spacing between the probes (d/s). The ratios were calculated as 1 (a/d) and 1 (d/s) for samples used. Thus, from Smits' tables the correction factor has a value of 1 (24). The electrical resistivity, ρ, can be then calculated using the following formula [40]:

$$\rho = CtR \tag{3}$$

where C is the correction factor, t is the thickness of the GDL and R is the measured electrical resistance. The electrical conductivity (σ) is the reciprocal of the electrical resistivity (ρ):

$$\sigma = \frac{1}{\rho} \tag{4}$$

The in-plane conductivity of 5 samples was measured, where each GDL sample was measured 5 times. The individual values of the resistance were then averaged.

PEFC performance testing

The MEA was assembled using a C2 Freudenberg carbon substrate as the anode GDL, where the fabricated dual-layer Toray GDLs were used as the cathode GDL. The MEA utilised a catalyst coated membrane as received (Fuel Cells Earth, UK) produced from Nafion 212, with platinum loading at both the cathode and anode of 0.4 mg/cm^2. The single cell measurements were conducted on a commercial fuel cell test station (BioLogic, France) with an electrode active area of 5 cm^2. For each of the MEAs assembled PEFC performance measurements were taken at 80 °C at a range of air and hydrogen relative humidity conditions (from 25% RH to 100% RH). Measurements were also taken with oxygen and hydrogen at 50% RH. The back pressure for the anode and cathode were 250 kPa and 230 kPa respectively, and the stoichiometry for anode and cathode was adjusted to $\lambda = 1.3$ and $\lambda = 1.5$ in accordance with the EU test protocols for single cell measurements for PEFC [41]. EIS measurements were taken at 0.6 V for each of the test conditions.

Results and discussion

Morphology

The morphology and the surface structure of the carbon substrate and the MPLs was visualised by Scanning Electron Microscopy (SEM). Fig. 1 is a series of SEM micrographs showing the surface structure of the MPL coated and the uncoated Toray substrates. Notable differences can be seen between the surface structure and morphology of the carbon black MPL and those derived from graphene. This morphological difference depends on the physical characteristics of the MPL material. The particle size of the two materials differs greatly; where the Nanene graphene nanoplatelets (GNP) are several orders of magnitude larger than the Vulcan carbon black particles, up to10μm and 50 nm respectively, as stated by the manufactures.

Due to van der Waals forces, carbon black nanoparticles agglomerate in the MPL to form a microporous "sponge-like" structure [42,43]. The agglomeration of the carbon black particles results in the distinctive micro-cracks which characterise the surface of G0 (Fig. 1b), the carbon black MPL; these are the result of shrinkage caused by solvent evaporation in the thermal treatment phase [44]. The presence of these cracks is typical of carbon black based MPLs and is frequently noted in the literature [44–46]. However, they are absent from all the graphene containing MPLs regardless of carbon black content (Fig. 1c–f). The visible cracking on the surface of the G0 and its absence in the other samples indicates that this phenomenon is present in MPLs comprised of a smaller particle size, and the inclusion of particles with larger dimensions prevents its occurrence. The presence of cracks on the MPL surface has been shown to influence the transport of water in the MEA by acting as liquid phase pathways diverting the water from the GDL [46,47]; however surface cracking of the MPL has also been related to reduced mechanical durability of the layer [48]. As such the impact of these cracks on the optimisation of cell performance remains unclear.

The micrographs of G30, G50 and 70 (Fig. 1c, d and e) indicate that the mixed compositions result in a similar morphology and microstructure, where the graphene nanoplates are encompassed in a conductive filler formed of the

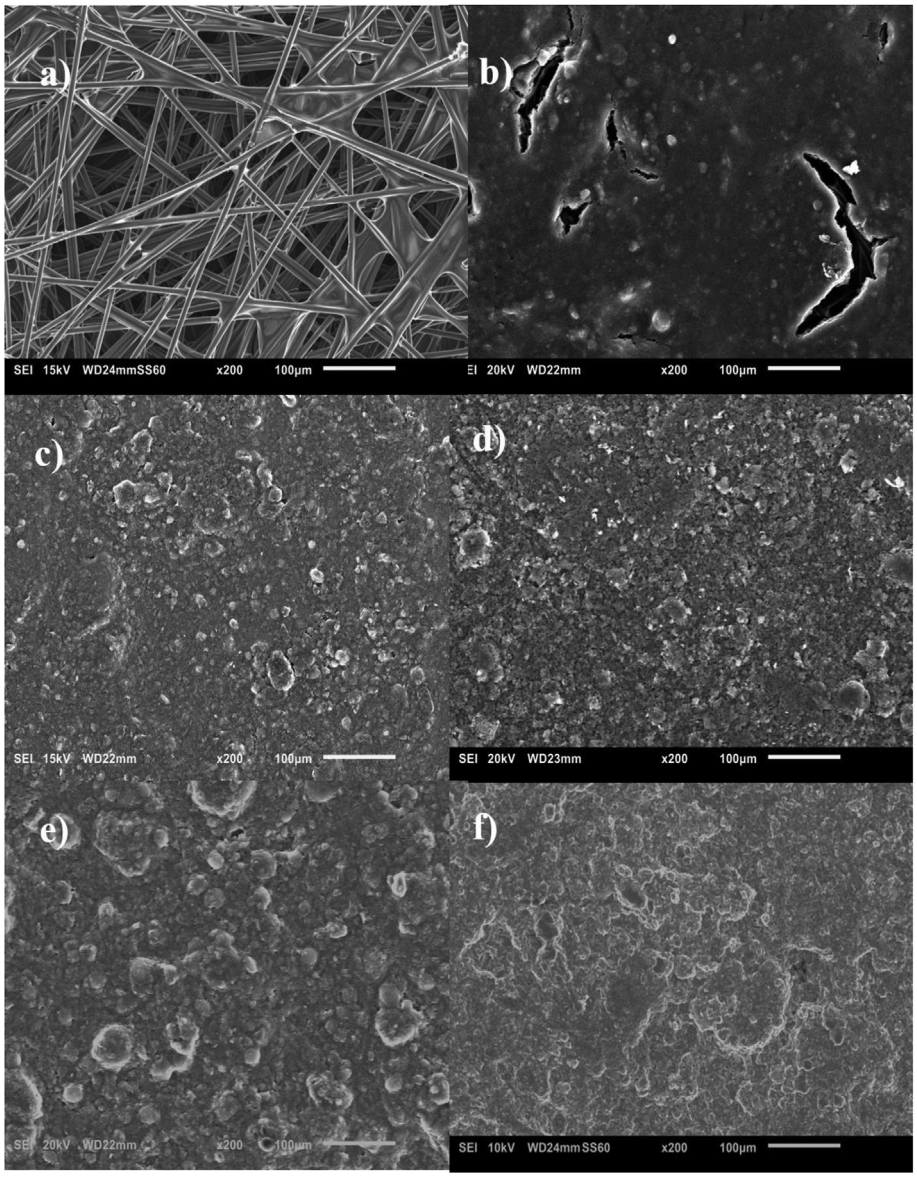

Fig. 1 – SEM micrographs of the dual-layer MPL coated and the uncoated GDLs (from top left to bottom right: Toray H-060, G0, G30, G50, G70 and G100). The number after the letter "G" represent the weight fraction of graphene in the MPL.

carbon black agglomerates. This is most easily distinguished in G30 (Fig. 1c), where stacked graphene platelets can be seen, alongside the sponge-like carbon black agglomerates with small surface cracks. While the graphene containing microporous layers visually appear smoother than the carbon black, when imaged with the SEM microscope it is apparent that they have a microscopic surface roughness owing to the dominant graphene which is decorated with the carbon black agglomerates. G30 (Fig. 1c) can be seen as being more densely packed than G50 and G70 (Fig. 1d and e) owing to the greater percentage of small particles in its composition. This influences the pore size distribution through the MPL, as can be seen in the following section (Fig. 3). G100 (Fig. 1f) is distinguishable from the other MPLs with a graphene inclusion due to its lack of conductive carbon black filler which results in a larger pore size.

Pore size distribution

The porosity and pore size distribution of the MPLs were obtained using MIP. For ease of identification and discussion of the microstructure, the pores of the single and dual-layer GDLs are classified into 3 groups according to their size, where: pores smaller than 0.07 μm are identified as micropores, mesopores range between the of 0.07–5 μm in size, and finally the pores larger than 5 μm are identified as macropores [45]. The determination of these groups is based on the mechanism for gas diffusion inside the pores, which differs depending on their size. Knudsen diffusion is the prevailing mechanism in the micropores whose dimensions are comparable to the gas mean free path, whereas bulk diffusion dominates in macropores. In mesopores, both bulk diffusion and Knudsen diffusion are present [49].

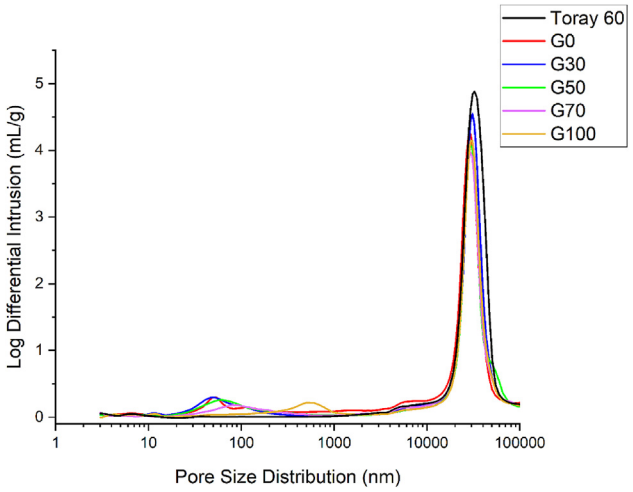

Fig. 2 – Pore size distribution of the uncoated and coated GDLs obtained by mercury intrusion porosimetry.

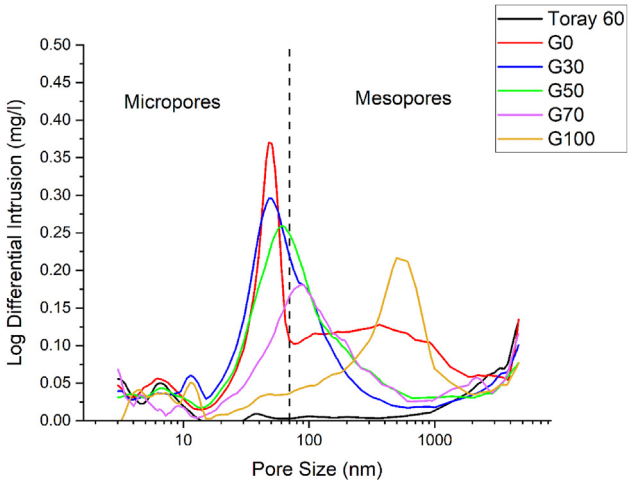

Fig. 3 – Pore size distributions of the microporous layer of the GDLs. The size of micropores is conventionally less than 70 nm and the size of the mesopores is between 70 and 5000 nm.

Mesopores are important for maintaining gas transmission in saturated conditions [50]. As the transport of liquid water typically takes place in pores larger than 20 μm [51], and due to the high capillary pressure the hydrophobic macropores become occupied by liquid water. The mesopores require an increased pressure to become filled by liquid water, and are both able to remove liquid water from the catalyst layer and provide pathways for gas transmission. Thus the presence of mesopores greatly enhances the ability of the reactant gas to maintain free transmission in the GDL. As such presence of mesopores in the GDL enhances the mass transport capabilities at higher current densities and in higher relative humidity conditions [50].

Fig. 2 shows the pore size distribution for the uncoated and dual-layer GDLs. Unsurprisingly, the uncoated GDL is mainly comprised of macropores which can be seen as the large peak after 10 μm, whereas the addition of the microporous layer to the GDL leads to the addition of micropores and mesopores to the pore profile. The composition of the microporous layers influences the pore profiles of the coated GDLs, where the peak pore size (within the region where the micropores and/or mesopores dominate) increases with the increasing inclusion of graphene in the MPL. The pore size distribution and porosity of the coated GDLs are mainly governed by the macroporous substrate and as such Fig. 3 was produced for ease of comparison of the microporous layers. This figure shows the distribution of the micropores and the mesopores and thus provides greater clarity when determining the variation in pore sizes in the microporous layer. G0 (the pure Vulcan carbon black MPL) has the typical pore profile of the conventional microporous layer, where the majority of the pores are in the microporous region with the sharp peak at around 50 nm. Conversely, G100 (the pure graphene MPL) has a larger average pore size, with most pores occurring in the mesoporous region and the peak occurring at 500 nm. The two materials were visualised using SEM and the average particle size was found to be 20–80 nm for Vulcan carbon black and 0.5–5 μm for graphene, both of which are within the range of the manufacturer's specifications. Given the average particle size of the two materials, it is unsurprising that the average pore size of G100 is an order of magnitude larger than that of G0.

The inclusion of GNP to the MPL composition increases the average pore sizes in the MPL; and leads to the formation of mesopores in the layer. Interestingly, for the mixed composition MPLs, Vulcan is the dominant material in determining the average pore size. Although G70 is largely comprised of graphene, its peak pore size is 83 nm, which is closer to that of G0 (50 nm) than that of G100 (500 nm). Likewise, G30 and G50 are characterised by micropores, with the most frequent pore size being the same for G30 (50 nm) as for G0. However, the distribution is more evenly weighted for G30, due to the inclusion of GNP. As G30 has a higher percentage of carbon black filler than G50 and G70, it has a larger number of micropores in the MPL. G50 MPL has what appears to be a desirable pore size distribution with a peak pore size of 61 nm. Namely, G50 has an even distribution of micropores and small mesopores and this may lead to enhanced performance at high relative humidity operation and current densities; enabling the simultaneous capillary wicking of liquid water to mitigate flooding at the cathode and improve reactant diffusion to the catalyst layer [52,53]. It is noteworthy that the G0 MPL has a peak within the micropores region and has also a good portion of mesopores that span over a wider range compared to other MPLs. This is most likely due to the relatively high tendency of the carbon black particles to form agglomerates during heat treatment process; this subsequently creates interspaces (i.e. pores) whose size span widely within the micropores and mesopores ranges.

Table 2 shows the cumulative pore volume of the investigated MPL-coated GDLs. It can be observed that G0 has the largest cumulative pore volume (1.82 ml g^{-1}) compared to the other samples. This is determined not only by the presence of micropores (which form as a result of agglomeration of carbon black particles) but also due to the cracks which were clearly visible in Fig. 1b. Table 2 also shows that the cumulative pore

Table 2 – The porosity and cumulative pore volume of the MPL coated GDLs.

Gas Diffusion Layer	Porosity	Cumulative Pore Volume (ml g^{-1})
G0	74%	1.82
G30	72%	1.71
G50	72%	1.71
G70	72%	1.62
G100	71%	1.56

volume in general decreases with increasing graphene content; increasing graphene content in the MPL from 30% (G30) or 50% (G50) to 100% (G100) decreases the cumulative pore volume from 1.71 to 1.56 ml g^{-1}.

The porosity is an important physical property as the porosity and diffusivity of the GDL determines its effective diffusivity. This is significant as diffusion is the main mode of gas transport in the GDL [54]. G0 has the highest porosity of the MPL coated GDLs and as such is likely to have a greater effective gas diffusivity than the other MPLs. Although, this does not account for the either the presence of the cracks, nor the influence of liquid water which could obstruct diffusive pathways and precipitate mass transport loss.

It should be noted that the decrease in porosity is disproportionate to the decrease in the cumulative pore volume. This could be attributed to the fact that the cumulative pore volume has been reported (by the software associated with the MIP instrument) in unit of volume per unit of mass rather than unit of volume per unit of volume. Due to "stacking" nature of the GNP, less void fraction is expected to be in a unit of mass with increasing GNP content.

Contact angle

The wettability, or hydrophobicity/hydrophilicity, of the MPLs is dependent on the physical properties of the material and the surface structure. This determines the strength of the interactions between the surface and the water molecules. Static contact angle measurements were used to investigate the wettability characteristics of the microporous layer surfaces. All of the GDL surfaces investigated were found to be hydrophobic, exhibiting a contact angle greater than 90°; see Fig. 4. The value of the contact angle of the uncoated carbon substrate (131°) shows that the surface of the uncoated substrate is moderately hydrophobic. This is in good agreement with those reported in the literature (129 ± 9°) [55]. The inclusion of 10 wt % of PTFE increases the hydrophobicity of the substrates compared to pure carbon fibre substrates.

Referring to Fig. 4, one is able to see that the addition of the microporous layers increases the contact angle of the uncoated Toray carbon substrate. This is largely due to the inclusion of PTFE (20 wt %) in their composition, as addition of the MPL reduces the surface roughness. The roughness of a surface impacts on the contact angle; where the rougher the surface, the larger the contact angle [55].

Similar contact angles were measured with 30% (151.6°), 50% (151.5°) and 100% (151.4°) GNP content. This corresponds to approximately a 15% increase in the contact angle of the uncoated Toray substrate. Moreover, G30 indicates that a 13% increase in the contact angle of the surface of GDL facing the catalyst layer can be achieved with even a small addition of graphene (30%) to the MPL. The inclusion of graphene into the MPL composition results in an increase in the contact angle comparative to the single material Vulcan MPL, an increase of around 3% for G30 and around 5% for G50, G70 and G100 respectively.

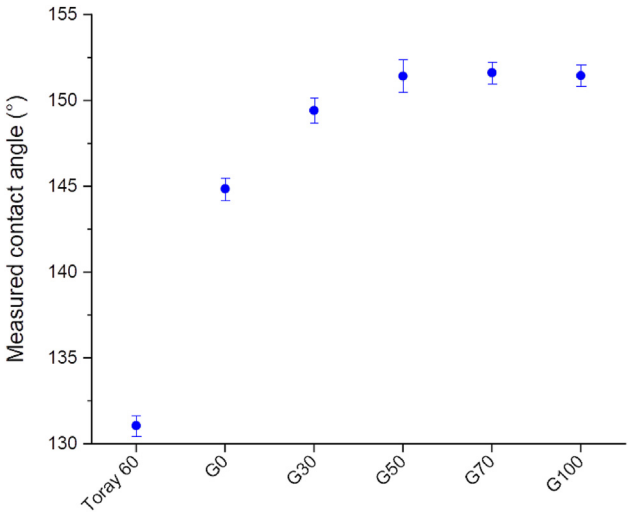

Fig. 4 – The measured static contact angle of water droplets on the coated and uncoated GDL. The error bars represent the 95% confidence.

The contact angle is determined by the physical characteristics and the morphology of the surface. As previously mentioned, the graphene nanoplatelets exhibit a stacking behaviour in the MPL; the slight increase in the contact angle of the MPLs composed with graphene is attributed to this stacked graphene morphology. This indicates that there are fewer pathways for the removal of water from the surface. Moreover, the surface morphology of G0 is characterised by cracks which serve as channels for water penetration. However, as there is minor variation in the measured contact angles of the graphene containing MPLs, it can be understood that the dominating factor in their wettability is the PTFE content, which is kept constant.

Through-plane permeability

Fig. 5 shows the through-plane permeability measurements of the uncoated and MPL coated GDLs. As can be expected, the uncoated carbon substrate has the highest through-plane permeability of those measured, which decreases by around 70% with the addition of the microporous layer. A significant drop in the through-plane permeability with the addition of the MPL has been widely observed in the literature [36,56].

A high permeability is desirable as it assists in transporting the reactant gases to the catalyst layer, and allows water produced at the catalyst to be directed to the flow channels to prevent electrode flooding. Low permeability increases reactant transport resistance and creates a higher-pressure gradient which may not be beneficial for driving excess liquid water away from the catalyst layer [36,39].

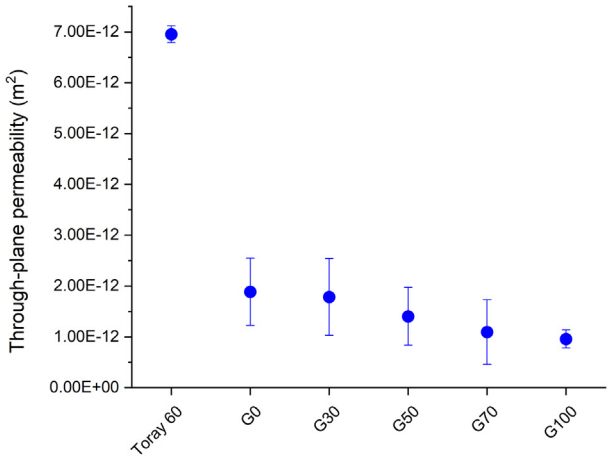

Fig. 5 – Through-plane permeability of the uncoated and dual layer GDLs. The error bars represent the 95% confidence.

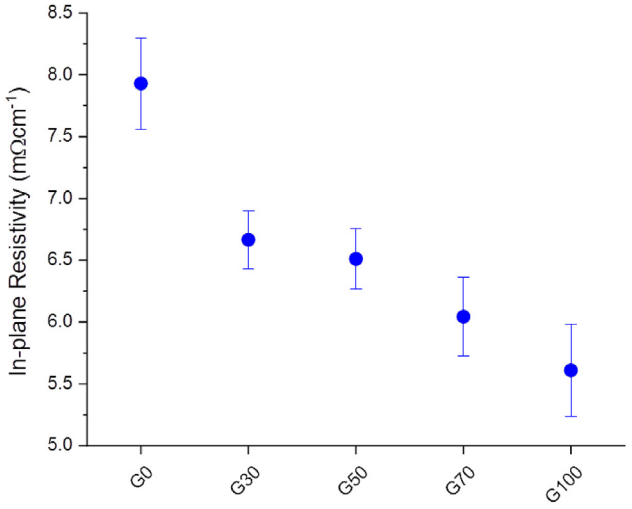

Fig. 6 – The measured in-plane resistivity of the MPL coated GDLs. The error bars represent the 95% confidence.

The permeability of the gas diffusion layer is dependent on its physical structure and morphology, notably the porosity and the pore size distribution. As was previously noted, these microstructural properties varied between the different MPL compositions, where the highest pore volume was reported with G0, and decreased with the addition of graphene to the layer. When comparing the microporous layers, it is important to emphasise that the PTFE composition and carbon loading of the MPL were kept consistent at 20 wt % and 2.0 mg cm^{-1} respectively, as is typically used in the literature. The addition of graphene to the MPL leads to a gradual decrease in the through-plane permeability which becomes more prominent with the increase in graphene content. Notably, G30 has minimal decrease in permeability amounting to a 1.5% reduction compared with the conventional MPL (G0), whereas G70 and G100 exhibit a much greater 48% and 55% decrease in the permeability, respectively. This reduction in through-plane permeability of the graphene based MPLs indicates that the inclusion of graphene in the MPL leads to a greater resistance to air flow which can be attributed to the morphology of the graphene flakes which differs greatly from that of the Vulcan carbon black particles. Namely, the graphene used have a 2-dimenisonal geometry as opposed to the spherical morphology of the carbon black particles. This 2-dimensional geometry lends to dense, horizontal stacking of the graphene flakes in the MPL, which forms a sheet-like structure and results in reduced pore volume (Table 2). This obstructs air flow in the through-plane direction, thus translating in reduced through-plane permeability with increasing graphene content. This is in agreement with [30] who reported a lower through-plane permeability for single material graphene MPL than those derived from carbon black. Notably, the single material MPLs have the smallest variation in permeability; this is attributed to the homogeneity of the microstructure.

In-plane electrical resistivity

Fig. 6 shows that the in-plane electrical resistivity measurements indicate that G100, the graphene based MPL, has a much lower in-plane resistivity than G0, the carbon black MPL, at 5.6 mΩ cm^{-1} and 8.0 mΩ cm^{-1} respectively. These values are in good agreement with those reported in Ref. [29] in which a similar grade of graphene nanoplatelets was used. The in-plane electrical resistivity of the uncoated Toray-60 GDL is not included in the graph as the measurement fluctuated however it was in the range of 12 to 9 mΩ cm^{-1}.

The excellent electron conductivity of graphene is widely acknowledged and reported in the literature, where single layer graphene has an exceptionally high electrical conductivity (6×10^5 S m^{-1}) [57]. The electrical conductivity of the graphene nanoplatelets is greatly influenced by the number of graphene layers, the lateral size, and the purity of the material [58–61]. To this end, few layer graphene has been used in a number of investigations involving nano-electronics, ultra-capacitors, gas sensors and catalyst supports [15,62].

The Nanene graphene nanoplatelets used in this investigation has a high purity of 98% and notably few layers (<5); the electrical conductivity of which exceeds that of the Vulcan XC 72 R carbon black used (~277 S m^{-1}) [34,63]. As the resistance of the MPL is dependent on the physical properties of the carbon material and its electrical conductivity when it is adhered to the PTFE, it is therefore unsurprising that the inclusion of graphene nanoplatelets in the MPL composition increases the conductivity of the surface for all MPLs tested. The measured resistivity of G30 indicates that even a small inclusion of graphene in the MPL (30%) has marked improvements on the electronic conduction of the layer, equating to a 20% reduction in resistivity from the conventional carbon black MPL. Higher inclusions of graphene lead to greater improvements in the electronic conduction of the MPL, where G50 and G70 have a 23% and 32% reduction in resistivity respectively compared to G0.

Fuel cell performance

Single cell performance tests were conducted under different humidity conditions, from low humidity operation (RH = 25%) to high humidity operation (RH = 100%). High humidity

operation can result in liquid water formation and accumulation, leading to what is conventionally known as 'water flooding' which impedes oxygen supply to the cathode catalyst layer, leading to mass transport losses and reduced catalyst efficiency [3,64]. On the other hand, low humidity conditions lead to membrane electrolyte dehydration, reducing ionic resistance of the membrane electrolyte and leading to increased ohmic losses [4,5,65]. Varying the operating conditions enables the assessment of the dominant mechanisms and phenomena for water transport in the MPL, and thus enabling the optimisation of the MPL for cell efficiency.

Polarisation curves were taken at a 25%, 50%, 75% and 100% relative humidity conditions in air, and also at 50% relative humidity in oxygen (Fig. 7a, b, c, d and e), at a constant temperature of 80 °C; this allowed for the assessment of the viability of the graphene-based MPLs under actual operating conditions.

The MPL coated GDLs perform better than the uncoated Toray-60 GDL in all conditions, which is consistent with previous research findings; the addition of the MPL reduces membrane dehydration in low humidity conditions [66,67] and at high humidity conditions reduces liquid water saturation at the catalyst layer-GDL interface [7,68]. Fig. 7a, shows the IV curves of the GDLs at 25% relative humidity operation. In these conditions, the G30 MPL generally outperforms all the other MPLs. Under low humidity operating conditions, the ohmic losses caused by the membrane dry-out is the prevailing factor behind the low performance of the fuel cell. The high performance exhibited by G30 indicates that it is better than the other MPLs at retaining liquid water and preventing membrane dry-out, particularly G100 which achieves noticeably lower potentials. However, at 50% RH (Fig. 7b), G30 and the G0 start to experience significant potential drops at a relatively intermediate current density of 1.2 A cm^{-2}. This could be attributed to the inability of the above MPLs to reject excess liquid water produced at the cathode catalyst layer. This trend continues at 75% and 100% RH operations, where liquid water is more prevalent; thus it is clear that these performance losses are due to the inability of G0 and G30 to sufficiently divert liquid water away from the cathode catalyst layer.

Larger inclusions of graphene in the MPL composition produce a higher limiting current density and greater power density in more humidified conditions (50%, 75% and 100% RH). Fig. 7b, c and d indicate that G50, G70 and G100 do not suffer the same potential drops that G0 and G30 experience in these conditions. It can be concluded that, under intermediate or high humidity conditions, the addition of 50% or above of graphene to the MPL has a positive impact on the fuel cell performance as evidenced from the lower mass transport losses and the increased limiting current density of the fuel cell. G100 in particular has the lowest limiting current density (1.97 A cm^{-2}) in the 25% RH humidity operation but exhibits the 2nd highest limiting current density in the 100% RH humidity condition, 2.17 A cm^{-2} (G50 is the highest at 2.25 W cm^{-2}). For G100 the highest performance was recorded at 75% RH where the peak power point of 0.90 W cm^{-2} was reached at 1.6 A cm^{-2}. This greatly exceeded that of G0 and G30 in these conditions (0.64 W cm^{-2} and 0.49 W cm^{-2}) and was higher than G70 and G50 at 0.85 W cm^{-2} and 0.87 W cm^{-2}, respectively. G50 performs well overall and records the highest power density at 50% RH, 0.91 W cm^{-2} at 1.9 A cm^{-2} (Fig. 8b). G50 produces the highest power density of all MPLs in 100% RH (0.88 W cm^{-2} at 1.7 A cm^{-2}). The pore size distribution data gives an indication of why this is the case. Namely, the peak pore size within the micropores and mesopores ranges was found to shift towards the mesopores range as the graphene content in the MPL increases, resulting, at the same time, in presence of less amount of micropores which typically trap liquid water in the catalyst layer. This condition (i.e. presence of higher amount of mesopores and less amount of micropores) enhances removal of liquid water away from the catalyst layer which explains why G50, G70 and G100 do not experience the same potential drops at high current densities which G30 and G0 experience.

Similar findings have been reported when other carbon based materials have been mixed with carbon black in the microporous layer, such as graphene [29–31], multiwall carbon nanotubes [10,12,53,69] which have led to the presence of mesopores in the microporous layer and have reduced mass transport losses at high current densities in high relative humidity operations.

Fig. 8e shows the polarisation curve at 50% relative humidity where pure oxygen was used as the oxidant; this significantly reduces the effect of mass transport losses and reveals the impact of resistance on cell performance. In these conditions G30 performs very well and has the lowest resistance of all of the GDLs resulting from a well hydrated membrane and good GDL conductivity. This is confirmed by the EIS results which can be seen in the following section (Fig. 9e). G50, G70 and G100 behave similarly in terms of resistance and cell performance is similar in this condition.

Overall, G50 is the optimal MPL composition under the commonly used intermediate and high humidity conditions as it produces high fuel cell performance with relatively low amount of graphene that is much more expensive than carbon black.

Electrochemical Impedance Spectrometry

Electrochemical Impedance Spectrometry (EIS) was performed at 0.6 V. Fig. 9 shows the results for the EIS measurements for the MEAs at 25%, 50%, 75% and 100% RH in air, as well as 50% RH in O_2. The results of the EIS correspond well with those obtained from the IV curves (Fig. 9). Fig. 9 a-d indicate that for the fuel cell operating in air the ohmic losses are comparable for all of the MPL coated GDLs this is evident from the intercepts of the respective curves with the x-axis which are similar for all the MPL coated GDLs. On the other hand, the uncoated GDL intercepts with the x-axis at a higher value, signifying a higher ohmic resistance compared to the MPL-coated GDLs particularly with 25% relative humidity condition. The ohmic resistance is the sum of all the contact resistances between the components and the bulk ohmic resistance of each component [70]. Typically, the membrane resistance accounts for the most of the ohmic resistance and is largely dependent on the level of humidification of the polymer membrane. The uncoated GDL clearly reduces the capability of the membrane to retain water and limits the contact between the GDL and catalyst layer. The

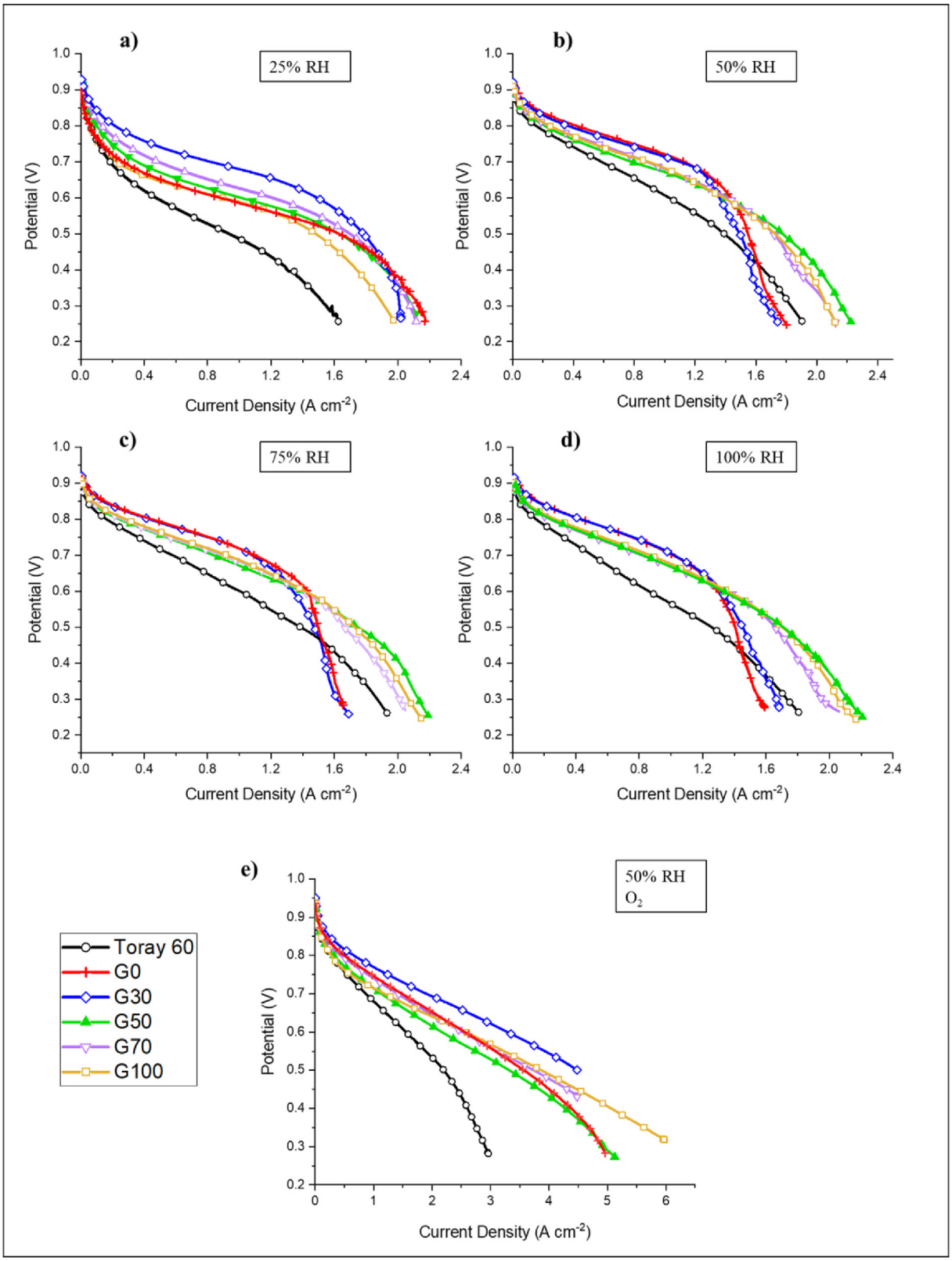

Fig. 7 – Polarisation curves of the fuel cell with MPL coated and uncoated GDLs at (a–e) 25%, 50%, 75% and 100% relative humidity in air, and 50% relative humidity in pure oxygen.

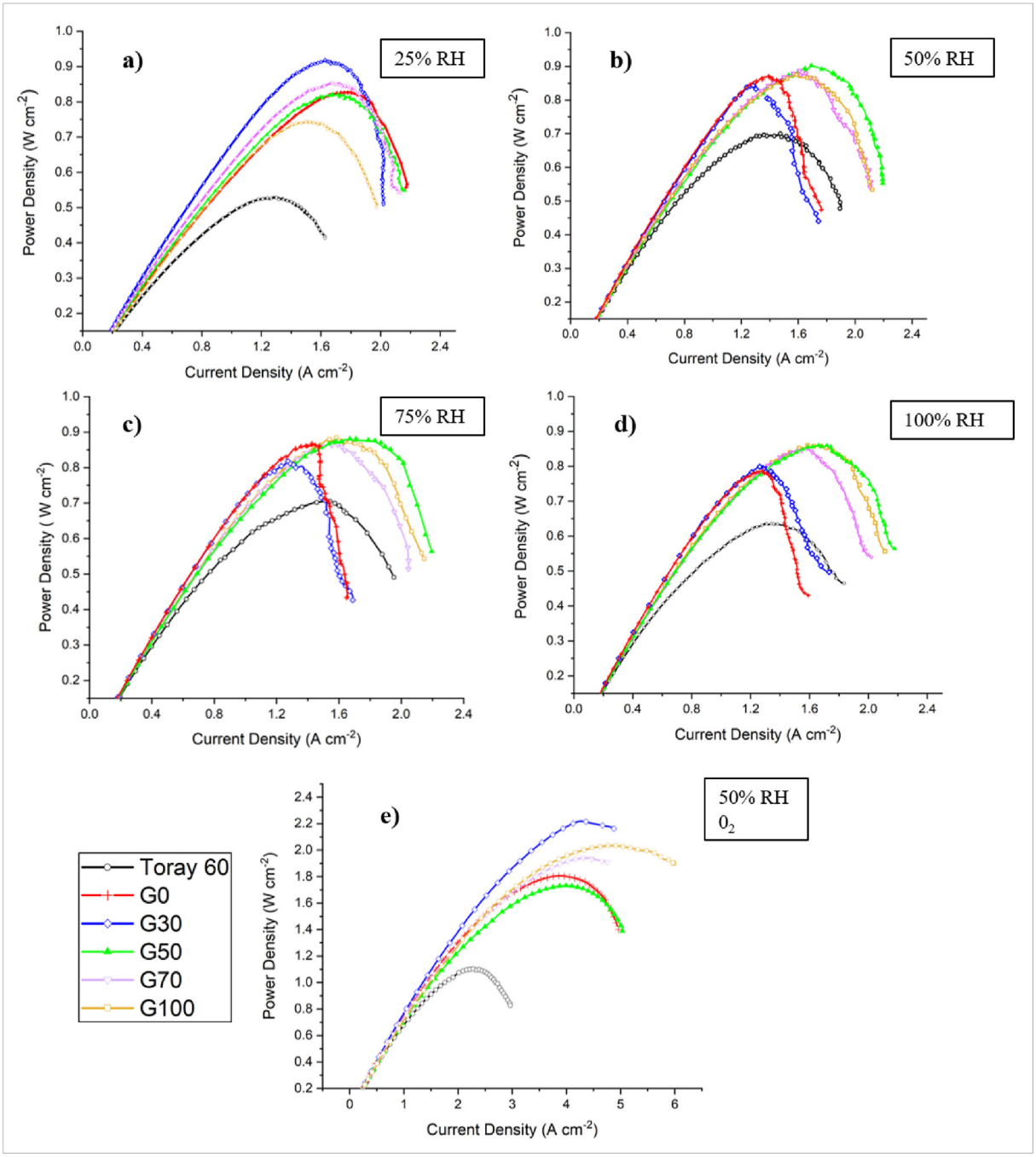

Fig. 8 – Power density measurements of the MPL coated gas diffusion layers in different conditions (a–e) 25%, 50%, 75% and 100% relative humidity.

ability of the MPL to enhance these two properties (i.e. electrical contact with the catalyst layer and water management) is well reported in the literature [71–76].

Typically, the first semi-circle in the EIS represents the charge transfer resistance (which signifies how dry/wet the triple phase boundary in the catalyst layer) while the second semi-circle represents the mass transport resistance. With air as an oxidant, these two semi-circles often overlap at conventionally-used voltages (e.g. 0.6 V) and it becomes rather uneasy to quantify the respective resistances. However, qualitatively, one could see that From Fig. 9 a-d, the MEAs with G50, G70 and G100 demonstrate significantly less mass transport resistance compared to those with G0 and G30 at relatively high humidity relative humidities (i.e. 50, 75 and 100%). This is in accordance with the corresponding polarisation curves shown in Fig. 8 b-d where the MEAs with G50, G70 and G100 features higher limiting current densities compared to those of G0 and G100. This signifies that the graphene content in the MPL should be more than 30% to have reasonable amount of mesopores (Fig. 3) and subsequently better water management under high humidity conditions. To isolate mass transport resistance and differentiate between

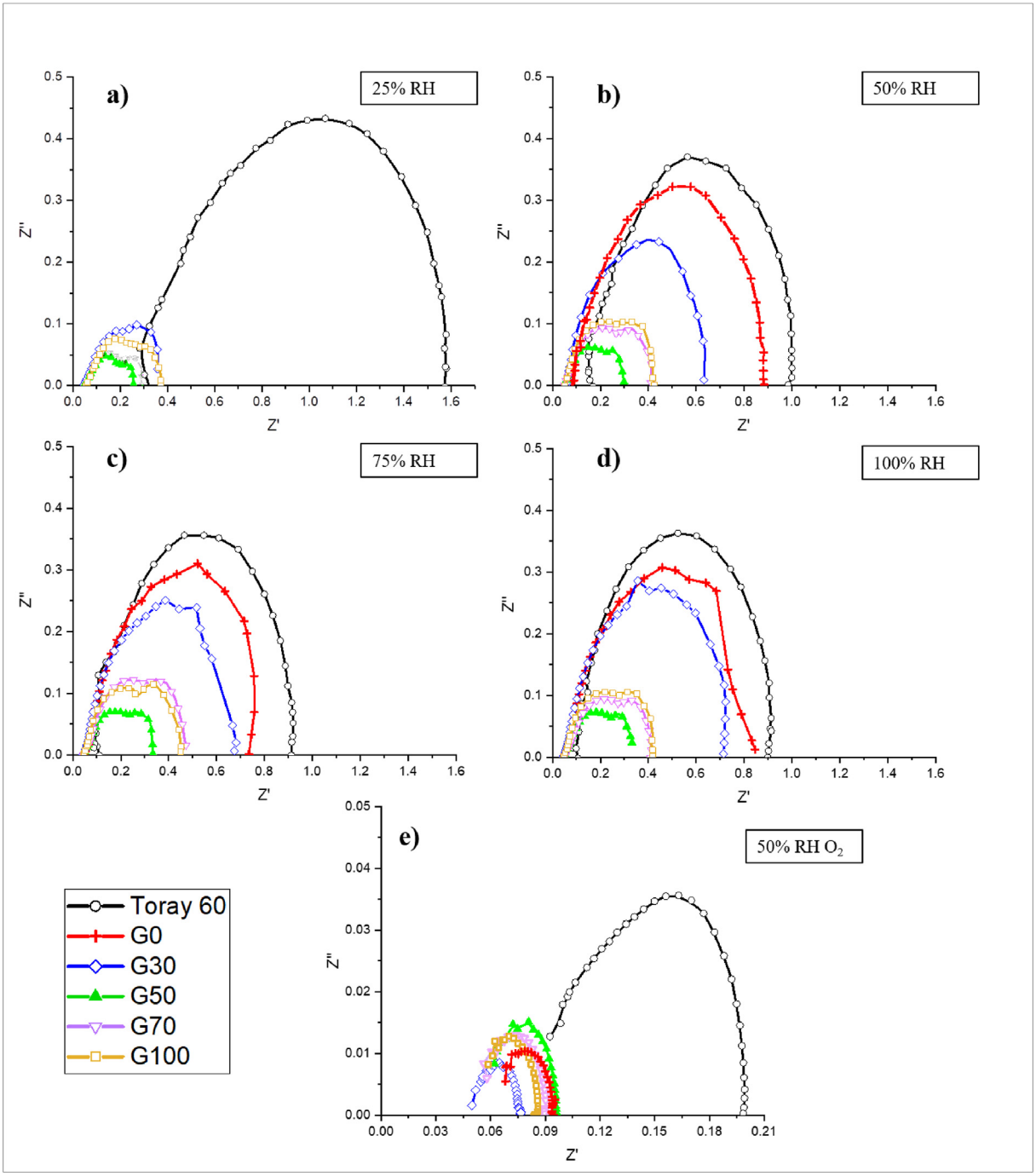

Fig. 9 – Electrical impedance spectrometry measurements taken at 0.6 V for the MPL coated and uncoated GDLs at (a–e) 25%, 50%, 75% and 100% relative humidity in air, and 50% relative humidity in pure oxygen.

the various MEAs in terms of charge transfer resistance, the fuel cell was run with pure oxygen as an oxidant (Fig. 9e). Excluding the curve of the uncoated GDL, the MEAs with G0 and G30 MPLs show less charge transfer resistance compared to other MEAs (i.e. those with G50, G70 and G100 MPLs) under a commonly-used humidity condition (50% RH). This indicates that a small amount of graphene in the MPL (e.g. 30%) is sufficient to obtain a good amount of micropores (Fig. 3) and therefore maintain a good humidification level of the catalyst layers under low or intermediate humidity conditions. This is in line with the respective curves shown in Fig. 7 where the IV curve G30 (and to a lesser degree G0) was shown to have better performance under low humidity conditions and/or under low/intermediate current density operation.

Conclusions

Microporous layers produced from graphene and carbon black in varying concentrations were applied to carbon paper GDLs.

The concentration of graphene in the MPL was varied to enhance MEA performance and to optimise their design for water management in high humidity conditions. Below are the main findings of the study:

- The polymer electrolyte membrane fuel cell was found to perform better with relatively low graphene content in the cathode MPL (≤30%) under low humidity conditions (e.g. 0 or 25% RH) and this is due the availability of high amount of micropores that assist in retaining water needed to humidify the membrane electrolyte and the membrane phase in the catalyst layer.
- Larger amounts of graphene (≥50%) are needed to be added to the cathode MPL for the fuel cells operating with intermediate or high humidity conditions (50, 75 or 100% RH). Such amounts are necessary to obtain fewer numbers of micropores and at the same time sufficient amounts of mesopores that are required to drive excess water away from the MEA and subsequently mitigate water flooding.
- Expectedly, the electrical conductivity of the MPL increases with increasing graphene content and this is evidently due to substantially higher electrical conductivity of graphene compared to carbon black. On the other hand, the gas permeability of the MPL-coated GDL was found to decreases with increasing graphene content; this is attributed to the sheet-like structure of the graphene used which hiders the flow of the gases.

Declaration of competing interest

The authors declare that they have no known competing financial interests or personal relationships that could have appeared to influence the work reported in this paper.

Acknowledgments

The first author would also like to thank the ESPRC CDT for Clean Fossil Energy and Carbon Capture Storage (EP/L016362/1) as well as the International Flame Research Foundation for their financial support.

REFERENCES

[1] Steele BCH, Heinzel A. Materials for fuel-cell technologies. 2001. Available: www.nature.com.
[2] Lee SJ, Kim SG, Park GG, Kim CS. Quantitative visualization of temporal water evolution in an operating polymer electrolyte fuel cell. Int J Hydrogen Energy 2010/10//2010;35(19):10457–63. https://doi.org/10.1016/j.ijhydene.2010.07.173.
[3] Deevanhxay P, Sasabe T, Tsushima S, Hirai S. In situ diagnostic of liquid water distribution in cathode catalyst layer in an operating PEMFC by high-resolution soft X-ray radiography. Electrochem Commun 2012/8//2012;22(1):33–6. https://doi.org/10.1016/j.elecom.2012.05.028.
[4] Yan Q, Toghiani H, Wu J. Investigation of water transport through membrane in a PEM fuel cell by water balance experiments. J Power Sources 2006/7//2006;158(1):316–25. https://doi.org/10.1016/j.jpowsour.2005.09.013.
[5] Ramani V, Kunz HR, Fenton JM. Investigation of Nafion®/HPA composite membranes for high temperature/low relative humidity PEMFC operation. J Membr Sci 2004/3//2004;232(1–2):31–44. https://doi.org/10.1016/j.memsci.2003.11.016.
[6] Zhou J, Shukla S, Putz A, Secanell M. Analysis of the role of the microporous layer in improving polymer electrolyte fuel cell performance. Electrochim Acta 2018/4//2018;268:366–82. https://doi.org/10.1016/j.electacta.2018.02.100.
[7] Qi Z, Kaufman A. Improvement of water management by a microporous sublayer for PEM fuel cells. 2002.
[8] Wang X, Zhang HM, Zhang JL, Xu HF, Tian ZQ, Chen J, Zhong HX, Liang YM, Li BL. A bi-functional micro-porous layer with composite carbon black for PEM fuel cells. J Power Sources 2006/11//2006;162(1):474–9. https://doi.org/10.1016/j.jpowsour.2006.06.064.
[9] Lin G, Liu S, Qu G, Song Y, Li T, Liu F, Hu Y. Effect of pore size distribution in the gas diffusion layer adjusted by composite carbon black on fuel cell performance. 2020. https://doi.org/10.1002/er.6350.
[10] Gharibi H, Javaheri M, Mirzaie RA. The synergy between multi-wall carbon nanotubes and Vulcan XC72R in microporous layers. Int J Hydrogen Energy 2010/9//2010;35(17):9241–51. https://doi.org/10.1016/J.IJHYDENE.2009.08.092.
[11] Gallo Stampino P, Omati L, Cristiani C, Dotelli G. Characterisation of nanocarbon-based gas diffusion media by electrochemical impedance spectroscopy. In: Fuel cells. 2 ed.10; 2010/4//2010. p. 270–7. https://doi.org/10.1002/fuce.200900126.
[12] Lin S-Y, Chang M-H. Effect of microporous layer composed of carbon nanotube and acetylene black on polymer electrolyte membrane fuel cell performance. Int J Hydrogen Energy 2015/6//2015;40(24):7879–85. https://doi.org/10.1016/J.IJHYDENE.2014.10.146.
[13] Najafab AT, Leeuwner MJ, Wilkinson DP, Gyenge EL. Electrochemically produced graphene for MicroporousLayers in fuel cells. ChemSusChem 2016;9:1689–97. 1689 –1697.
[14] Leeuwner MJ, Wilkinson DP, Gyenge EL. Novel graphene foam microporous layers for PEM fuel cells: interfacial characteristics and comparative performance. Fuel Cell 2015/12//2015;15(6):790–801. https://doi.org/10.1002/fuce.201500031.
[15] Avouris P, Xia F. Graphene applications in electronics and photonics. MRS Bull 2012;37:1225–34.
[16] Lee FC, Ismail MS, Ingham DB, Hughes KJ, Ma L, Lyth SM, Pourkashanian M. Alternative architectures and materials for PEMFC gas diffusion layers: a review and outlook. Renew Sustain Energy Rev 2022/9//2022;166. https://doi.org/10.1016/J.RSER.2022.112640. 112640–112640.
[17] Alnaqbi H, Sayed ET, Al-Asheh S, Bahaa A, Alawadhi H, Abdelkareem MA. Current progression in graphene-based membranes for low temperature fuel cells. Int J Hydrogen Energy 2022/5//2022. https://doi.org/10.1016/J.IJHYDENE.2022.03.255.
[18] Devrim Y, Bulanık Durmuş GN. Composite membrane by incorporating sulfonated graphene oxide in polybenzimidazole for high temperature proton exchange membrane fuel cells. Int J Hydrogen Energy 2022/2//2022;47(14):9004–17. https://doi.org/10.1016/J.IJHYDENE.2021.12.257.
[19] Gahlot S, Kulshrestha V. Graphene based polymer electrolyte membranes for electro-chemical energy applications. Int J Hydrogen Energy 2020/7//2020;45(34):17029–56. https://doi.org/10.1016/J.IJHYDENE.2019.06.047.
[20] Lv J, Tongxiang L, Chen W. The effects of molybdenum and reduced graphene oxide on corrosion resistance of amorphous nickel–phosphorus as bipolar plates in PEMFC

environment. Int J Hydrogen Energy 2016/6//2016;41(23):9738–45. https://doi.org/10.1016/J.IJHYDENE.2016.03.104.
[21] Wang J, Min L, Fang F, Zhang W, Wang Y. Electrodeposition of graphene nano-thick coating for highly enhanced performance of titanium bipolar plates in fuel cells. Int J Hydrogen Energy 2019/6//2019;44(31):16909–17. https://doi.org/10.1016/J.IJHYDENE.2019.04.245.
[22] Witpathomwong S, Okhawilai M, Jubsilp C, Karagiannidis P, Rimdusit S. Highly filled graphite/graphene/carbon nanotube in polybenzoxazine composites for bipolar plate in PEMFC. Int J Hydrogen Energy 2020/11//2020;45(55):30898–910. https://doi.org/10.1016/J.IJHYDENE.2020.08.006.
[23] Arbizzani C, Righi S, Soavi F, Mastragostino M. Graphene and carbon nanotube structures supported on mesoporous xerogel carbon as catalysts for oxygen reduction reaction in proton-exchange-membrane fuel cells. Int J Hydrogen Energy 2011/4//2011;36(8):5038–46. https://doi.org/10.1016/J.IJHYDENE.2011.01.083.
[24] Daş E, Alkan Gürsel S, Işikel Şanli L, Bayrakçeken Yurtcan A. Comparison of two different catalyst preparation methods for graphene nanoplatelets supported platinum catalysts. Int J Hydrogen Energy 2016/6//2016;41(23):9755–61. https://doi.org/10.1016/J.IJHYDENE.2016.01.111.
[25] Devrim Y, Arıca ED, Albostan A. Graphene based catalyst supports for high temperature PEM fuel cell application. Int J Hydrogen Energy 2018/6//2018;43(26):11820–9. https://doi.org/10.1016/J.IJHYDENE.2018.03.047.
[26] Arici E, Kaplan BY, Mert AM, Alkan Gursel S, Kinayyigit S. An effective electrocatalyst based on platinum nanoparticles supported with graphene nanoplatelets and carbon black hybrid for PEM fuel cells. Int J Hydrogen Energy 2019/5//2019;44(27):14175–83. https://doi.org/10.1016/J.IJHYDENE.2018.11.210.
[27] Jafri RI, Rajalakshmi N, Dhathathreyan KS, Ramaprabhu S. Nitrogen doped graphene prepared by hydrothermal and thermal solid state methods as catalyst supports for fuel cell. Int J Hydrogen Energy 2015/4//2015;40(12):4337–48. https://doi.org/10.1016/J.IJHYDENE.2015.02.008.
[28] Marinoiu A, Carcadea E, Sacca A, Carbone A, Sisu C, Dogaru A, Raceanu M, Varlam M. One-step synthesis of graphene supported platinum nanoparticles as electrocatalyst for PEM fuel cells. Int J Hydrogen Energy 2021/3//2021;46(22):12242–53. https://doi.org/10.1016/J.IJHYDENE.2020.04.183.
[29] Leeuwner MJ, Patra A, Wilkinson DP, Gyenge EL. Graphene and reduced graphene oxide based microporous layers for high-performance proton-exchange membrane fuel cells under varied humidity operation. J Power Sources 2019/5//2019;423:192–202. https://doi.org/10.1016/J.JPOWSOUR.2019.03.048.
[30] Ozden A, Shahgaldi S, Zhao J, Li X, Hamdullahpur F. Assessment of graphene as an alternative microporous layer material for proton exchange membrane fuel cells. Fuel 2018/3//2018;215:726–34. https://doi.org/10.1016/J.FUEL.2017.11.109.
[31] Mariani M, Latorrata S, Patrignani S, Gallo Stampino P, Dotelli G. Characterization of novel graphene-based microporous layers for Polymer Electrolyte Membrane Fuel Cells operating under low humidity and high temperature. Int J Hydrogen Energy 2020/2//2020;45(11):7046–58. https://doi.org/10.1016/j.ijhydene.2019.12.213.
[32] Chen J, Bailey JJ, Britnell L, Perez-Page M, Sahoo M, Zhang Z, Strudwick A, Hack J, Guo Z, Ji Z, Martin P, L Brett DJ, R Shearing P, Holmes SM. The performance and durability of high-temperature proton exchange membrane fuel cells enhanced by single-layer graphene. Nano Energy 2022/3//2022;93. https://doi.org/10.1016/J.NANOEN.2021.106829. 106829–106829.
[33] Latorrata S, Gallo Stampino P, Scandola L, Cristiani C, Dotelli G. Analysis of degradation mechanisms and durability assessment of graphene-based MPLs for PEM fuel cells. ECS Trans 2018/7//2018;86(13):337–45. https://doi.org/10.1149/08613.0337ecst.
[34] Pérez-Rodríguez S, Pastor E, Lázaro MJ. Electrochemical behavior of the carbon black Vulcan XC-72R: influence of the surface chemistry. Int J Hydrogen Energy 2018/4//2018;43(16):7911–22. https://doi.org/10.1016/j.ijhydene.2018.03.040.
[35] Simon C, Kartouzian D, Müller D, Wilhelm F, Gasteiger HA. Impact of microporous layer pore properties on liquid water transport in PEM fuel cells: carbon black type and perforation. J Electrochem Soc 2017;164(14):F1697–711. https://doi.org/10.1149/2.1321714jes.
[36] Orogbemi OM, Ingham DB, Ismail MS, Hughes KJ, Ma L, Pourkashanian M. Through-plane gas permeability of gas diffusion layers and microporous layer: effects of carbon loading and sintering. J Energy Inst 2018/4//2018;91(2):270–8. https://doi.org/10.1016/J.JOEI.2016.11.008.
[37] Ismail MS, Hughes KJ, Ingham DB, Ma L, Pourkashanian M. Through-plane permeability for untreated and PTFE-treated gas diffusion layers in proton exchange membrane fuel cells. J Fuel Cell Sci Technol 2010/10//2010;7(5):510161–7. https://doi.org/10.1115/1.4000685.
[38] Ismail MS, Borman D, Damjanovic T, Ingham DB, Pourkashanian M. On the through-plane permeability of microporous layer-coated gas diffusion layers used in proton exchange membrane fuel cells. Int J Hydrogen Energy 2011;36. https://doi.org/10.1016/j.ijhydene.2010.09.012. 16 ed.
[39] Ismail MS, Damjanovic T, Ingham DB, Pourkashanian M, Westwood A. Effect of polytetrafluoroethylene-treatment and microporous layer-coating on the electrical conductivity of gas diffusion layers used in proton exchange membrane fuel cells. J Power Sources 2010/5//2010;195(9):2700–8. https://doi.org/10.1016/J.JPOWSOUR.2009.11.069.
[40] Smits FM. Measurement of sheet resistivities with the four-point probe. Bell Syst Technical J 1958;37(3):711–8. https://doi.org/10.1002/j.1538-7305.1958.tb03883.x.
[41] Tsotridis G, Pilenga A, De Marco G, Malkow T, C. European Commission. Joint Research, EU harmonised test protocols for PEMFC MEA testing in single cell configuration for automotive applications. Publications Office; 2015.
[42] Wang XL, Zhang HM, Zhang JL, Xu HF, Tian ZQ, Chen J, Zhong HX, Liang YM. Micro-porous layer with composite carbon black for PEM fuel cells. Electrochim Acta 2006/6//2006;51(23):4909–15. https://doi.org/10.1016/J.ELECTACTA.2006.01.048.
[43] Park S, Lee J-W, Popov BN. A review of gas diffusion layer in PEM fuel cells: materials and designs. Int J Hydrogen Energy 2012/4//2012;37(7):5850–65. https://doi.org/10.1016/J.IJHYDENE.2011.12.148.
[44] Chen Z, Pan W, Yao D, Gao M, Gao Y, Chen X, Krzywanski J, Wang F. Crack evolution during the film drying process of fuel cell microporous layer ink. Colloids Surf A Physicochem Eng Asp 2022/10//2022;650. https://doi.org/10.1016/J.COLSURFA.2022.129283. 129283–129283.
[45] Fishman Z, Bazylak A. Heterogeneous through-plane porosity distributions for treated PEMFC GDLs. II. Effect of MPL cracks. J Electrochem Soc 2011;158(8). https://doi.org/10.1149/1.3594636. B846–B846.
[46] Markötter H, Alink R, Haußmann J, Dittmann K, Arlt T, Wiede F, Tötzke C, Klages M, Reiter C, Riesemeier H, Scholta J, Gerteisen D, Banhart J, Manke I. Influence of cracks in the microporous layer on the water distribution in a PEM fuel cell investigated by synchrotron radiography. Electrochem Commun 2013/9//2013;34:22–4. https://doi.org/10.1016/J.ELECOM.2013.04.006.

[47] Markötter H, Alink R, Haußmann J, Dittmann K, Arlt T, Wiede F, Tötzke C, Klages M, Reiter C, Riesemeier H, Scholta J, Gerteisen D, Banhart J, Manke I. Visualization of the water distribution in perforated gas diffusion layers by means of synchrotron X-ray radiography. Int J Hydrogen Energy 2012/5//2012;37(9):7757–61. https://doi.org/10.1016/j.ijhydene.2012.01.141.
[48] Chun JH, Jo DH, Kim SG, Park SH, Lee CH, Kim SH. Improvement of the mechanical durability of micro porous layer in a proton exchange membrane fuel cell by elimination of surface cracks. Renew Energy 2012/12//2012;48:35–41. https://doi.org/10.1016/J.RENENE.2012.04.011.
[49] Kast W, Hohenthanner CR. Mass transfer within the gas-phase of porous media. Int J Heat Mass Tran 2000/3//2000;43(5):807–23. https://doi.org/10.1016/S0017-9310(99)00158-1.
[50] Chen J, Xu H, Zhang H, Yi B. Facilitating mass transport in gas diffusion layer of PEMFC by fabricating micro-porous layer with dry layer preparation. J Power Sources 2008/8//2008;182(2):531–9. https://doi.org/10.1016/j.jpowsour.2008.04.031.
[51] Li T, Li T, Wang K, Wang J, Liu Y, Han Y, Song J, Hu H, Lin G, Lui Y. Preparation of hierarchical-pore gas diffusion layer for fuel cell. 2020. https://doi.org/10.1007/s10853-019-04323-9.
[52] Tanuma T, Kawamoto M, Kinoshita S. Effect of properties of hydrophilic microporous layer (MPL) on PEFC performance. J Electrochem Soc 2017;164(6):F499–503. https://doi.org/10.1149/2.0371706jes.
[53] Fan CC, Chang MH. Improving proton exchange membrane fuel cell performance with carbon nanotubes as the material of cathode microporous layer. Int J Energy Res 2016/2//2016;40(2):181–8. https://doi.org/10.1002/er.3445.
[54] Ismail MS, Hughes KJ, Ingham DB, Ma L, Pourkashanian M. Effects of anisotropic permeability and electrical conductivity of gas diffusion layers on the performance of proton exchange membrane fuel cells. Appl Energy 2012/7//2012;95:50–63. https://doi.org/10.1016/J.APENERGY.2012.02.003.
[55] El-kharouf A, Mason TJ, Brett DJL, Pollet BG. Ex-situ characterisation of gas diffusion layers for proton exchange membrane fuel cells. J Power Sources 2012/11//2012;218:393–404. https://doi.org/10.1016/J.JPOWSOUR.2012.06.099.
[56] Williams MV, Kunz HR, Fenton JM. Influence of convection through gas-diffusion layers on limiting current in PEM FCs using a serpentine flow field. J Electrochem Soc 2004;151(10). https://doi.org/10.1149/1.1789791. A1617–A1617.
[57] Du X, Skachko I, Barker A, Andrei EY. Approaching ballistic transport in suspended graphene. Nat Nanotechnol 2008;3(8):491–5. https://doi.org/10.1038/nnano.2008.199.
[58] Fang XY, Yu XX, Zheng HM, Jin HB, Wang L, Cao MS. Temperature- and thickness-dependent electrical conductivity of few-layer graphene and graphene nanosheets. Phys Lett 2015/10//2015;379(37):2245–51. https://doi.org/10.1016/J.PHYSLETA.2015.06.063.
[59] Nirmalraj PN, Lutz T, Kumar S, Duesberg GS, Boland JJ. Nanoscale mapping of electrical resistivity and connectivity in graphene strips and networks. Nano Lett 2011/1//2011;11(1):16–22. https://doi.org/10.1021/nl101469d.
[60] Rouhi N, Wang YY, Burke PJ. Ultrahigh conductivity of large area suspended few layer graphene films. Appl Phys Lett 2012/12//2012;101(26). https://doi.org/10.1063/1.4772797.
[61] Tan YW, Zhang Y, Stormer HL, Kim P. Temperature dependent electron transport in graphene. Eur Phys J: Spec Top 2007/9//2007;148(1):15–8. https://doi.org/10.1140/epjst/e2007-00221-9.
[62] Caradonna A, Badini C, Padovano E, Pietroluongo M. Electrical and thermal conductivity of epoxy-carbon filler composites processed by calendaring. Materials 2019;12(9). https://doi.org/10.3390/ma12091522.
[63] Tang S, Tang S, Sun G, Qi J, Sun S, Guo J, Xin ang Q. Review of new carbon materials as catalyst supports in direct alcohol fuel cells. Chin J Catal 2010/1//2010;31(1):12–7. https://doi.org/10.1016/s1872-2067(09)60034-6.
[64] Hickner MA, Siegel NP, Chen KS, Hussey DS, Jacobson DL, Arif M. In situ high-resolution neutron radiography of cross-sectional liquid water profiles in proton exchange membrane fuel cells. J Electrochem Soc 2008;155(4). https://doi.org/10.1149/1.2826287. B427–B427.
[65] Cho MK, Park H-Y, Lee SY, Lee B-S, Kim H-J, Henkensmeier D, Yoo S-J, Kim J-Y, Han J, Park HS, Sung J-E, Jang JH. Effect of catalyst layer ionomer content on performance of intermediate temperature proton exchange membrane fuel cells (IT-PEMFCs) under reduced humidity conditions. 2016. https://doi.org/10.1016/j.electacta.2016.12.009.
[66] Kang K, Ju H. Numerical modeling and analysis of micro-porous layer effects in polymer electrolyte fuel cells. J Power Sources 2009/12//2009;194(2):763–73. https://doi.org/10.1016/j.jpowsour.2009.05.046.
[67] Chen G, Zhang G, Guo L, Liu H. Systematic study on the functions and mechanisms of micro porous layer on water transport in proton exchange membrane fuel cells. Int J Hydrogen Energy 2016/3//2016;41(9):5063–73. https://doi.org/10.1016/j.ijhydene.2016.01.074.
[68] Tseng CJ, Lo SK. Effects of microstructure characteristics of gas diffusion layer and microporous layer on the performance of PEMFC. Energy Convers Manag 2010/4//2010;51(4):677–84. https://doi.org/10.1016/j.enconman.2009.11.011.
[69] Lee J, Lee J, Banerjee R, George MG, Muirhead D, Shrestha P, Liu H, Ge N, Chevalier S, Bazylak A. Multiwall carbon nanotube-based microporous layers for polymer electrolyte membrane fuel cells. J Electrochem Soc 2017;164(12):F1149–57. https://doi.org/10.1149/2.0861712jes.
[70] Wu J, Yuan XZ, Wang H, Blanco M, Martin JJ, Zhang J. Diagnostic tools in PEM fuel cell research: Part I Electrochemical techniques. Int J Hydrogen Energy 2008;33:1735–46. Pergamon.
[71] Weber AZ. Improved modeling and understanding of diffusion-media wettability on polymer-electrolyte-fuel-cell performance. J Power Sources 2010. https://doi.org/10.1016/j.jpowsour.2010.03.011.
[72] Weber AZ, Newman J. Effects of microporous layers in polymer electrolyte fuel cells. J Electrochem Soc 2005;152(4). https://doi.org/10.1149/1.1861194. A677–A677.
[73] Park G-G, Sohn Y-J, Yang T-H, Yoon Y-G, Lee W-Y, Kim C-S. Effect of PTFE contents in the gas diffusion media on the performance of PEMFC. J Power Sources 2004/5//2004;131(1–2):182–7. https://doi.org/10.1016/J.JPOWSOUR.2003.12.037.
[74] Park S, Lee J-W, Popov BN. Effect of carbon loading in microporous layer on PEM fuel cell performance. J Power Sources 2006/12//2006;163(1):357–63. https://doi.org/10.1016/J.JPOWSOUR.2006.09.020.
[75] Ye D, Gauthier E, Benziger JB, Pan M. Bulk and contact resistances of gas diffusion layers in proton exchange membrane fuel cells. J Power Sources 2014/6//2014;256:449–56. https://doi.org/10.1016/j.jpowsour.2014.01.082.
[76] Ferreira RB, Falcão DS, Oliveira VB, Pinto AMFR. Experimental study on the membrane electrode assembly of a proton exchange membrane fuel cell: effects of microporous layer, membrane thickness and gas diffusion layer hydrophobic treatment. Electrochim Acta 2017/1//2017;224:337–45. https://doi.org/10.1016/j.electacta.2016.12.074.